

# Numerical subgap spectroscopy of double quantum dots coupled to superconductors

Rok Žitko

*Jožef Stefan Institute, Jamova 39, SI-1000 Ljubljana, Slovenia*

*and Faculty of Mathematics and Physics, University of Ljubljana, Jadranska 19, SI-1000 Ljubljana, Slovenia*

(Received 22 December 2014; revised manuscript received 24 March 2015; published 9 April 2015)

Double quantum dot nanostructures embedded between two superconducting leads or in a superconducting ring have complex excitation spectra inside the gap which reveal the competition between different many-body phenomena. We study the corresponding two-impurity Anderson model using the nonperturbative numerical renormalization group (NRG) technique and identify the characteristic features in the spectral function in various parameter regimes. At half-filling, the system always has a singlet ground state. For large hybridization, we observe an inversion of excited interdot triplet and singlet states due to the level repulsion between two subgap singlet states. The Shiba doublet states split in two cases: (a) at nonzero superconducting phase difference and (b) away from half-filling. The most complex structure of subgap states is found when one or both dots are in the valence fluctuation regime. Doublet splitting can lead to a parity-changing quantum phase transition to a doublet ground state in some circumstances. In such cases, we observe very different spectral weights for the transitions to singlet or triplet excited Shiba states: the triplet state is best visible on the valence-fluctuating dot, while the singlets are more pronounced on the half-filled dot.

DOI: [10.1103/PhysRevB.91.165116](https://doi.org/10.1103/PhysRevB.91.165116)

PACS number(s): 72.10.Fk, 72.15.Qm, 75.75.-c, 74.78.-w

## I. INTRODUCTION

The advances in fabrication and characterization of small electronic devices have enabled new ways to perform spectroscopy of strongly correlated electron systems. A prominent example is the tunneling spectroscopy [1–4] of interacting quantum dots coupled to superconducting contacts as well as magnetic adatoms on superconducting surfaces [5–9], where the competition between the Kondo screening [10] and superconducting correlations can be studied in exquisite detail because it engenders spectroscopically sharp resonances known as the Andreev bound states (or Yu-Shiba-Rusinov states or simply Shiba states) [11–20]. At low enough temperatures even fine details can be resolved [8,9,21,22] and in some cases quantitative agreement is found between the experiment and accurate theoretical modeling using nonperturbative numerical techniques [23].

The most thoroughly studied problem is that of a single quantum dot in the deep Kondo limit where charge fluctuations are frozen out and the device behaves essentially as a local moment characterized by a single bare parameter, the Kondo exchange coupling  $J_K$ , and at low temperatures by a single scaling parameter, the Kondo temperature  $T_K$ . When such a quantum dot (QD) is coupled to a superconducting host with energy gap  $\Delta$ , the ground state of the system depends on the ratio  $T_K/\Delta$ . For  $T_K \ll \Delta$ , the Kondo screening is incomplete due to a lack of quasiparticle states at low energy scales, thus the system behaves as a free local moment decoupled from the BCS bath, which is an overall spin doublet state. For  $T_K \gg \Delta$ , the Kondo screening is fully completed on energy scales high above the onset of pairing; the superconducting state is thus formed out of the local Fermi liquid state resulting from the Kondo effect, and is an overall spin singlet. For  $T_K \sim \Delta$  there is a quantum phase transition between these two different ground states. In this parameter range, the many-particle spectrum usually includes at least three states (one singlet and one doublet) below the onset of the continuum of quasiparticle states at  $\Delta$ . The singlet-doublet excitations are

spectroscopically visible as resonance pairs at  $\omega = \pm(E_S - E_D)$ . Additional complexity in the problem is brought about by nonzero difference of the superconducting phases that leads to Josephson current. The direction of the current depends on the subgap states and the singlet-doublet transitions can be directly related to the physics of 0 or  $\pi$  junction behavior [19,20,24].

Recently this research direction has intensified with a focus on more complex systems. Double quantum dots (DQD) are the minimal nontrivial systems that capture the essence of extended strongly correlated materials described by lattice models [25–30]. Coupled to superconducting leads, DQDs can serve to explore the competing effects of exchange coupling, charge fluctuations, Kondo screening, and superconductivity [31–34]. In this work, DQDs are studied using a reliable nonperturbative numerical renormalization group technique in a wide parameter range with the goal of identifying the characteristic behavior of the subgap Shiba states in various regimes, both their positions and spectral weights. The states are analyzed in terms of the eigenstates of the superconducting atomic (wide-gap) limit; the deviations between this simple theory and the full numerical calculations are pointed out. In the context of superconducting rings, an important question is the variation of the subgap state energies as a function of the flux. Strong flux dependence implies sizable particle exchange between the superconducting contacts on either side of the DQD structure, thus the regimes of enhanced valence fluctuations away from the integer filling limit are particularly interesting.

This work is structured as follows. In Sec. II we introduce the model, the numerical method, and the wide-gap approximation. The presentation of the results in Sec. III is divided into three subsections: the left-right symmetric case at (A) half-filling and (B) away from half-filling, and (C) the fully generic case with unequal quantum dots. Section IV contains a short discussion of the two-impurity Kondo quantum phase transition in the presence of superconductivity.

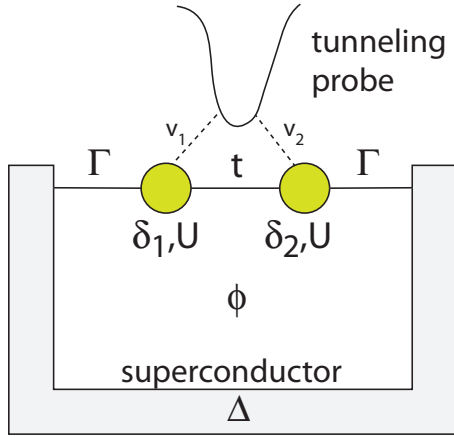


FIG. 1. (Color online) Schematic representation of the system: double quantum dot coupled to superconducting leads forming a ring pierced by the magnetic flux. The tunneling probe is very weakly coupled to either or both quantum dots.

## II. MODEL AND METHOD

The DQD system is schematically represented in Fig. 1. We consider two quantum dots ( $i = 1, 2$ ) described by the Anderson impurity model:

$$\begin{aligned} H_i &= \epsilon_i n_i + U n_{i\uparrow} n_{i\downarrow} \\ &= \delta_i (n_i - 1) + \frac{U}{2} (n_i - 1)^2 + \text{const.} \end{aligned} \quad (1)$$

Here  $n_i = n_{i\uparrow} + n_{i\downarrow}$  with  $n_{i\sigma} = d_{i\sigma}^\dagger d_{i\sigma}$  as the QD occupancy,  $U$  is the Hubbard charge repulsion, and  $\delta_i$  is the impurity energy level measured with respect to the particle-hole symmetric point (half-filling), i.e.,  $\delta_i = \epsilon_i + U/2$ . Each dot is coupled to a separate superconducting bath

$$H_{\text{SC},i} = \sum_{k\sigma} \epsilon_{k,i} c_{k\sigma,i}^\dagger c_{k\sigma,i} - \sum_{k\sigma} \Delta_i e^{i\phi_i} c_{k,\uparrow,i}^\dagger c_{-k,\downarrow,i} + \text{H.c.}, \quad (2)$$

where  $\epsilon_{k,i}$  is the band dispersion,  $\Delta_i$  is the gap parameter, and  $\phi_i$  is the superconducting phase. The difference of phases will be denoted as  $\phi = \phi_1 - \phi_2$ . The coupling terms are

$$H_{c,i} = \sum_{k\sigma} V_{k,i} d_{i\sigma}^\dagger c_{k\sigma,i} + \text{H.c.}, \quad (3)$$

where  $V_{k,i}$  is the hopping parameter. We assume that the two bands are flat: in the absence of superconductivity they have constant density of states  $\rho = 1/2D$  on the interval  $[-D : D]$ , thus  $D$  is one half of the bandwidth ( $D$  will henceforth be used as the energy unit,  $D = 1$ ). The hybridization strengths are characterized by functions

$$\Gamma_i(\omega) = \sum_k |V_{k,i}|^2 \delta(\omega - \epsilon_{k,i}) = \pi \rho V_i^2, \quad (4)$$

which will be taken as constants. The two dots are interconnected by a tunneling term

$$H_{12} = -t \sum_{\sigma} d_{1\sigma}^\dagger d_{2\sigma} + \text{H.c.} \quad (5)$$

Furthermore, two nearby quantum dots are typically also coupled capacitively [35–43] leading to an interdot Coulomb interaction term of the form

$$H_V = V n_1 n_2.$$

Most results presented in this work are calculated for

$$U/D = 0.27, \quad \Gamma/D = 0.02, \quad \Delta/D = 0.01, \quad V/D = 0, \quad (6)$$

while  $\delta_i$  and  $t$  will be variable. Exceptions to this parameter set will be clearly pointed out. For reference, the results for the normal state ( $\Delta = 0$ ) are presented as Supplemental Material [44].

Since  $U/\pi\Gamma \approx 4.3$ , the dots are in the Kondo regime near half-filling. This choice of parameters is experimentally realistic. The Kondo temperature (according to Wilson's definition) of each separate QD is given by [10,45]

$$T_K = 0.182U \sqrt{\rho J_K} \exp\left[-\frac{1}{\rho J_K}\right], \quad (7)$$

where

$$\rho J_K = \frac{2\Gamma}{\pi} \left( \frac{1}{U/2 - \delta} + \frac{1}{U/2 + \delta} \right). \quad (8)$$

At  $\delta = 0$  this gives  $T_K \approx 10^{-4} \ll \Delta$ . The ground state of a single quantum dot would be a doublet, with the excited singlet state at energy  $\approx 0.6\Delta$  [44].

The method of choice for this class of problems is the numerical renormalization group (NRG) [15,45–54] which is able to quantitatively reproduce the experimental results [23,55–58], but also provides additional detailed information about the system properties which are difficult or impossible to measure. The calculations were performed in the low-temperature limit with the discretization parameter  $\Lambda = 4$ , keeping 5000 states at each diagonalization step, with  $N_z = 2$  discretization meshes [59–62]. The only symmetry in the problem is the SU(2) spin symmetry. The spectra are computed using the density-matrix NRG algorithm [63] with the  $N/N + 1$  patching approach and with a mixed broadening scheme: for  $|\omega| > \Delta$  log-Gaussian broadening kernel with  $\alpha = 0.6$  is used, while for  $|\omega| < \Delta$  Gaussian broadening with  $\sigma = 10^{-3}$  is used (this latter choice mimics nonzero lifetime of resonances due to intrinsic relaxation processes at nonzero temperatures [9] and due to the presence of the tunneling probe [64]).

The spectral function of dot  $i$  is defined as

$$A_i(\omega) = -\frac{1}{\pi} \text{Im} G_i(\omega + i\delta), \quad (9)$$

where  $G_i(z) = \langle\langle d_{i\sigma}; d_{i\sigma}^\dagger \rangle\rangle_z$  is the local Green's function. Spectra are measurable by tunneling spectroscopy using weakly coupled additional normal-state or superconducting probes at finite bias voltage [8,21]. Finite bias drives the system out of equilibrium. In this work, it is assumed that the coupling is sufficiently weak ( $\Gamma_N/\Gamma_S \ll 1$ ), that the nonequilibrium effects may be neglected, and that the transport properties may be approximated using equilibrium spectral functions (i.e., the system remains in the linear response regime). For stronger coupling of the probe, different transport regimes become dominant [9,65–67].

Another quantity of interest is the interdot spectral function

$$A_{12}(\omega) = -\frac{1}{\pi} \text{Im} G_{12}(\omega + i\delta), \quad (10)$$

where  $G_{12}(z) = \langle \langle d_{1\sigma}; d_{2\sigma}^\dagger \rangle \rangle_z$ , which quantifies interdot correlations of the excitations. If the tunneling probe is coupled to both dots, the resulting spectrum is proportional to

$$\text{Im}[|v_1|^2 G_1(z) + |v_2|^2 G_2(z) + v_1^* v_2 G_{12}(z) + v_1 v_2^* G_{21}(z)]_{z=\omega+i\delta}, \quad (11)$$

providing access to the information contained in  $G_{12}$ . Here  $v_1$  and  $v_2$  are the tunnel couplings of the probe to either QD. Such a situation occurs in the experiments described in Refs. [21,23], where the segment of the carbon nanotube actually hosts two QDs and the probe is attached near the center of the tube.

At a qualitative level the structure of the subgap many-particle spectra can be described in the superconducting atomic limit (also known as the wide-gap limit) [15,18,68,69]. It consists of taking  $\Delta$  to infinity at a constant width of the conduction band. This limit is different from the related zero-bandwidth limit [69,70], where  $\Delta$  is kept constant and the conduction-band width is reduced to zero (i.e., the band is replaced by a single representative site). The wide-gap limit eliminates the continuum of the quasiparticle levels above the gap and the sole remaining effect of each lead is the proximity pairing term of the form  $\Gamma d_{i\uparrow}^\dagger d_{i\downarrow}^\dagger + \text{H.c.}$  We thus obtain a two-site discrete model with the following Hamiltonian:

$$H = \sum_i \delta_i (n_i - 1) + \frac{U}{2} \sum_i (n_i - 1)^2 + \sum_i (\Gamma e^{i\phi_i} d_{i\uparrow}^\dagger d_{i\downarrow}^\dagger + \text{H.c.}) - t \sum_\sigma (d_{1\sigma}^\dagger d_{2\sigma} + \text{H.c.}), \quad (12)$$

which can be easily diagonalized. The Kondo correlations due to quasiparticle states above the superconducting gap are fully excluded in this description, thus the results are quantitatively quite different compared to the accurate NRG calculations, especially when the role of the Kondo effect is increased either by increasing  $\Gamma$  or by decreasing  $\Delta$ . Furthermore, this method tends to overemphasize the BCS character of singlet states at the expense of the Kondo character in the exact solution. Nevertheless, the consecutive order of the lowest levels mostly match the observed subgap Shiba states. A systematic method for improving perturbatively upon the superconducting atomic limit has been described in Ref. [18]. Some further details are in the Supplemental Material [44].

### III. RESULTS

#### A. Left-right symmetric case, half-filling

We first consider the case of two equal dots at half-filling,  $\delta_1 = \delta_2 = 0$ , see Fig. 2. In Fig. 2(a) we plot the local spectral function  $A_1(\omega) = A_2(\omega)$  in the frequency range inside and around the gap,  $\omega \sim \Delta$ . In Fig. 2(b) we plot the interdot spectral function  $A_{12}(\omega)$ , which reveals the transition from Kondo to the antiferromagnetic regime at  $t \sim 10^{-2}$ , corresponding to  $J \sim T_K$ , then from the antiferromagnetic

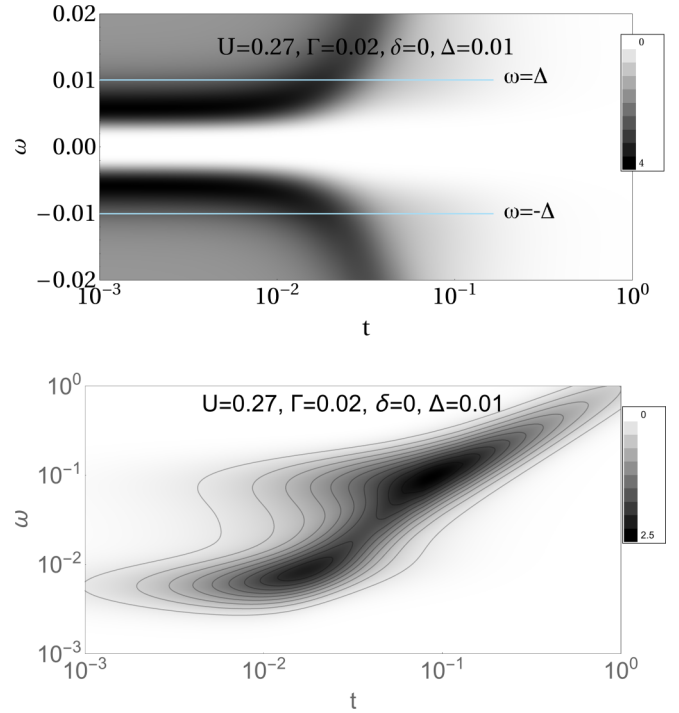


FIG. 2. (Color online) Left-right symmetric DQD system at half-filling. (a) Local spectral function  $A_1(\omega)$ . (b) Interdot spectral function  $A_{12}(\omega)$ : We plot the positive frequency part on a logarithmic scale.

to the molecular-orbital regime at  $t \sim 10^{-1}$ , corresponding to  $J \sim t$ .

For small  $t$  the subgap peaks appear close to the energy  $\Omega \approx 0.6\Delta$  of the excitations in the single-dot case [44]. While for a single dot the ground state is a doublet and the excited state a singlet, for two QDs the lowest-lying many-particle states are generated by combining two doublet states into a singlet and a triplet that are split at low  $t$  by  $J \approx 4t^2/U$  due to the interdot superexchange coupling. The ground state is always a singlet at half-filling. The singlet-triplet transition is not spectroscopically visible as it violates the  $\Delta S_z = \pm 1/2$  sum rule. Its presence is, however, revealed by a direct calculation of the many-particle spectrum using the numerical renormalization group, see the bottom-most panel in Fig. 3.

In the wide-gap limit [Eq. (12)] the triplet state  $|T\rangle = d_{1\uparrow}^\dagger d_{2\uparrow}^\dagger |0\rangle$  always has zero energy. There are five singlet states, four of which have energy of order  $U$  for  $t, \delta \ll U$ . The remaining singlet state  $|S1\rangle$  represents the interdot singlet and it has energy  $\approx -4t^2/U$  for low  $t$ , while at high  $t$  it is better described as the molecular orbital state with two electrons in the bonding orbital. In the wide-gap limit, the state  $|S1\rangle$  is the ground state at  $\delta = 0$  for all values of  $t$ .

The resonances in the spectral function  $A_1(\omega)$  reveal the excited doublet states. There are, in fact, two exactly degenerate doublets. This degeneracy is broken in the presence of the flux and away from half-filling as we show in the following subsections. In the  $t \rightarrow 0$  limit, these spectral peaks are exactly the same excitations as the doublet-singlet Shiba resonances in the single-dot case. They persist to finite  $t$ , although their energy is affected by the interdot coupling. The shift of the resonance is quadratic for  $t$  around  $10^{-2}$ . This is the region associated with the competition between the

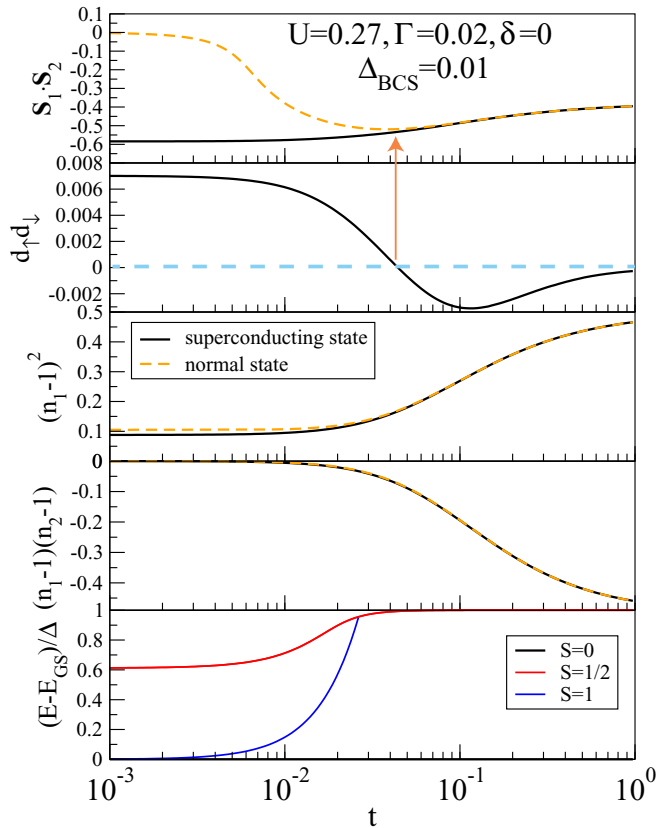


FIG. 3. (Color online) Expectation values and Shiba state energies in the left-right symmetric DQD system at half-filling. Results, where applicable, are shown for both normal-state and superconducting leads. The arrow indicates the point where the on-site pairing changes sign and the spin-spin correlations in the superconducting and normal-state cases start to deviate.

Kondo screening and the superexchange ( $T_K \sim J$ ) [44]. The NRG results show that the doublet-singlet energy difference is mostly driven by the downward shift of the singlet ground state which undergoes significant changes as a function of  $t$ , as also revealed by the evolution of the ground-state expectation values, in particular the spin  $\langle \mathbf{S}_1 \cdot \mathbf{S}_2 \rangle$  and pairing correlations  $\langle d_{1\uparrow} d_{1\downarrow} \rangle$ , see Fig. 3.

An important difference between the normal-state and superconducting case is found for the spin correlation  $\langle \mathbf{S}_1 \cdot \mathbf{S}_2 \rangle$  in the small  $t$  limit. In the normal case, the Kondo screening wins over the superexchange and each dot is screened individually, leading to  $\langle \mathbf{S}_1 \cdot \mathbf{S}_2 \rangle \rightarrow 0$ . In the superconducting case, the Kondo screening cannot be completed due to the lack of quasiparticles, thus the two unscreened moments are free to form a tightly bound local singlet state and  $\langle \mathbf{S}_1 \cdot \mathbf{S}_2 \rangle$  attains values close to the saturation ( $-0.6$ ). It is also revealing to observe that the difference in  $\langle \mathbf{S}_1 \cdot \mathbf{S}_2 \rangle$  between the two cases starts to grow near the point where the pairing correlations  $\langle d_{1\uparrow} d_{1\downarrow} \rangle$  change sign, as indicated by the arrow in Fig. 3. This is yet another sign that the Kondo screening becomes ineffective for  $t$  lower than this limiting value. Due to nonzero electron hopping in the model, this passing through zero is a simple crossover, not a quantum phase transition.

In the opposite limit of very large  $t$ , the behavior can be described in terms of molecular orbitals. In fact, from Fig. 3 it

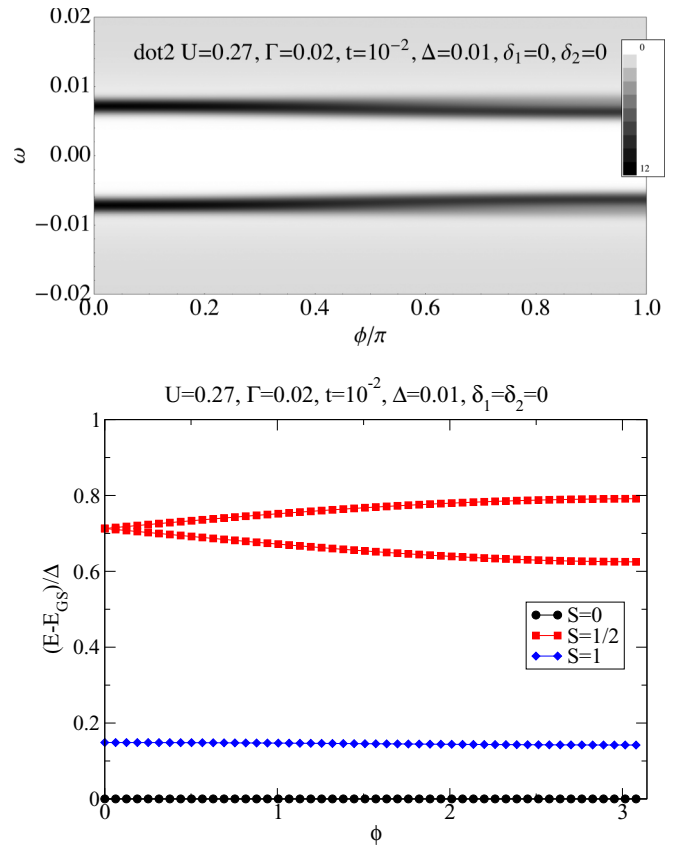


FIG. 4. (Color online) Spectral function  $A_1(\omega)$  and the diagram of the subgap Shiba states for  $\delta = 0$  as a function of the superconducting phase difference  $\phi$ .

is immediately obvious that in this limit there is little difference between the normal state and the superconducting case, since the superconducting gap is positioned in the region of low spectral density between the bonding and antibonding orbitals, thus it is ineffective. This is also signaled by the pairing correlations  $\langle d_{1\uparrow} d_{1\downarrow} \rangle$  going to zero for large  $t$ .

While the spin degrees of freedom are significantly affected by the superconductivity, the charge fluctuations are approximately the same in both the normal and superconducting case, as evidenced by nearly overlapping results for the interdot charge fluctuations  $\langle (n_1 - 1)(n_2 - 1) \rangle$  and only slightly reduced intradot charge fluctuations  $\langle (n_1 - 1)^2 \rangle$  in the superconducting state in the Kondo and antiferromagnetic regimes. The small reduction is due to the opening of the gap in the density of states and the corresponding reduction of electron hopping.

### 1. Flux dependence

We now study the effect of the difference in the superconducting phase (i.e., flux through the ring)  $\phi$ . We show the results for an intermediately strong  $t = 10^{-2}$  in Fig. 4. The flux induces a *splitting of the doublet Shiba states* which are otherwise degenerate at half-filling. At small  $\phi$  the splitting in the superconducting atomic limit is

$$\frac{t\Gamma^2}{\Gamma^2 + t^2} \phi. \quad (13)$$

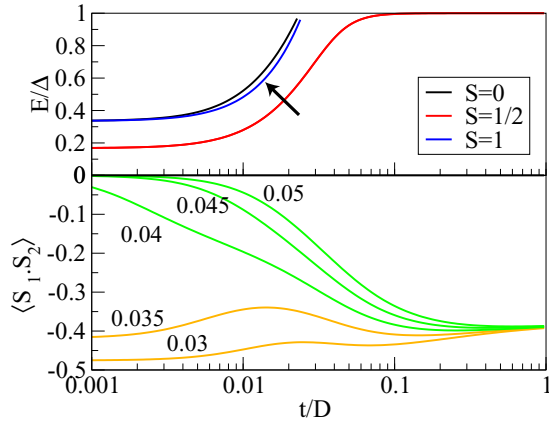


FIG. 5. (Color online) Dependence on the hybridization strength  $\Gamma$  in the left-right symmetric case at half-filling. (a) Subgap Shiba states for  $\Gamma = 0.045$ . The arrow brings to attention that the interdot triplet Shiba state is below the interdot singlet state. (b) Spin correlation function  $\langle \mathbf{S}_1 \cdot \mathbf{S}_2 \rangle(t)$  for a range of  $\Gamma$  (indicated near the corresponding curves) across the singlet-singlet crossover at  $\Gamma_t \approx 0.04$ .

The NRG results also show proportionality to  $t$  and  $\phi$  when both are small. The splitting is approximately sinusoidal and largest for  $\phi = \pi$ . In the spectral function, the splitting is actually only faintly visible because of the very unequal spectral weights: exactly at half-filling, only the lower energy doublet state appears in the spectra. The singlet-triplet splitting is hardly affected by nonzero  $\phi$ , there is only a slight downward trend in the energy difference, see the bottom panel in Fig. 4.

## 2. $\Gamma$ dependence

We now discuss the role of the hybridization  $\Gamma$ . In a single QD, the doublet-singlet transition occurs for  $\Gamma = \Gamma_t \approx 0.04$ . In the DQD system, with increasing  $\Gamma$ , the doublet excited states decrease in energy and at  $\Gamma \approx 0.025$  an additional excited singlet also enters the subgap region. This trend continues until  $\Gamma = \Gamma_t$ , where in the limit  $t \rightarrow 0$  we find degeneracy of five multiplets: two singlets, two (degenerate) doublets, and the triplet. For  $\Gamma > \Gamma_t$ , the nature of the singlet ground state changes, since it is associated with two separate Kondo clouds, rather than with the interdot singlet induced by the superexchange coupling. Consequently, in this range the triplet state lies close to the *excited* singlet state, rather than the ground state, see Fig. 5(a) where the subgap states are plotted for  $\Gamma = 0.0045 > \Gamma_t$ . Curiously, the interdot triplet is *lower* in energy than the interdot singlet state, although the superexchange coupling would lead to the opposite order. In the wide-gap limit, the triplet is indeed above the singlet. A simple interpretation is based on a three level model with two singlets and a triplet:

$$\begin{pmatrix} \epsilon_{S1} & 0 & \alpha \\ 0 & \epsilon_T & 0 \\ \alpha & 0 & \epsilon_{S2} \end{pmatrix}, \quad (14)$$

with  $\epsilon_T - \epsilon_{S1} = J = 4t^2/U$ , such that the coupling between the singlets  $\alpha$  is (much) larger than  $J$ . In this case a similar phenomenology is found, with the triplet state moving from

a value above the ground-state singlet to a value below the excited singlet as  $\epsilon_{S2} - \epsilon_{S1}$  changes sign, as happens at  $\Gamma = \Gamma_t$ . Numerical results indicate that  $\alpha \propto t$ , thus the requirement  $\alpha \gg J$  is fulfilled for the relevant range of  $t$ .

A further difference between the  $\Gamma < \Gamma_t$  and  $\Gamma > \Gamma_t$  regimes is manifest in the  $t$  dependence of  $\langle \mathbf{S}_1 \cdot \mathbf{S}_2 \rangle$  on the approach to the decoupled-dot  $t \rightarrow 0$  limit, see Fig. 5(b).

In the superconducting atomic limit, this transition corresponds to the transition from the interdot singlet state  $|S1\rangle$  with energy  $\approx -4t^2/U$  to the on-site-singlets state  $|S2\rangle$  with energy  $\approx U - 2\Gamma$ . The wide-gap limit does not distinguish between BCS and Kondo singlets, thus  $|S2\rangle$  has characteristics of a state with strong on-site BCS pairing, but at finite  $\Delta$  the NRG results show that the corresponding many-particle state should rather be described as two separate Kondo clouds. It should also be noted that this is a true transition only strictly at  $t = 0$ . For finite  $t$ , it is a smooth crossover.

Irrespective of the value of  $\Gamma$  and of the nature of the ground-state singlet, we find that the excited singlet state always monotonously increases in energy with  $t$  and the spectral functions are qualitatively always very similar. There are no quantum phase transitions between singlets as a function of  $t$ . This issue is discussed further in Sec. IV where the model without particle hopping but only exchange interaction is studied: that model has a true quantum phase transition.

## 3. $V$ dependence

We now discuss the effects of the interdot capacitive coupling  $V$  at half-filling. For moderate  $V \lesssim U$ , the effect of  $V$  is only quantitative and rather weak. As  $V$  increases, there is an increase in energy of the double-occupancy integer-spin Shiba states (seen through a decreasing energy of the excitation to the odd-occupancy half-spin, i.e., doublet, Shiba state), and an enhancement of the exchange coupling  $J$ :

$$J = \frac{1}{2} [\sqrt{(U-V)^2 + 16t^2} - (U-V)] \approx \frac{4t^2}{U-V}. \quad (15)$$

Both tendencies are visible in the numerical results in Fig. 6. At  $V = U$ , the system enters a phase with increased symmetry and enhanced Kondo temperature in the normal state if the interdot tunneling  $t$  is small, while for  $V > U$  the electrons tend to localize on a single site and form “local charge singlets” in the charge-ordering regime [35,71,72]. In the superconducting case at finite  $t$ , these trends are visible as a crossover at  $V \sim U$ . Although there is no change of the ground state, its nature changes significantly. For  $V \gg U$ , the lowest energy Shiba state is characterized by near zero spin correlations  $\langle \mathbf{S}_1 \cdot \mathbf{S}_2 \rangle \sim 0$ , large interdot charge fluctuations  $\langle (n_1 - 1)(n_2 - 1) \rangle \rightarrow -1$ , and negative on-site pairing  $\langle d_{i\uparrow} d_{i\downarrow} \rangle < 0$ . These are indeed the signatures of the charge-ordering regime. For large  $V$ , there is a single Shiba excited state inside the gap, which is also of local charge singlet kind. The excitation energy in fact corresponds to the splitting between the  $\frac{1}{\sqrt{2}}(|2,0\rangle \pm |0,2\rangle)$  eigenstates, which is equal to the isospin exchange coupling

$$J_{\text{iso}} = \frac{4t^2}{V-U}, \quad (16)$$

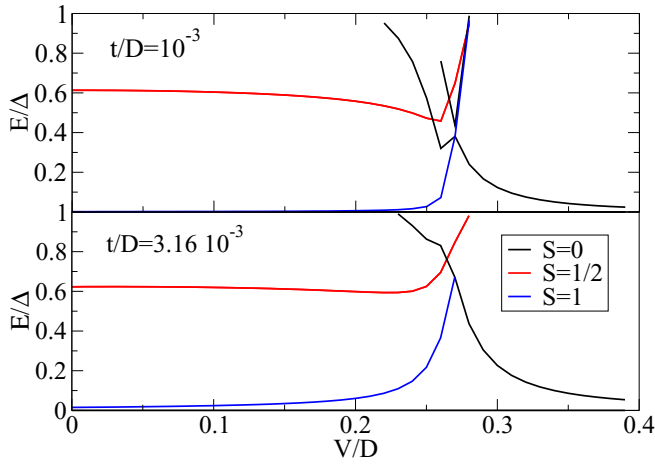


FIG. 6. (Color online) Dependence on the interdot capacitive coupling at half-filling.

and decreases with increasing  $V$ . Close to the crossover point at  $V \sim U$ , the behavior is particularly complex for small  $t$ ; see the case of  $t/D = 10^{-3}$ , upper panel in Fig. 6. In this case we even observe three subgap singlet states, which is a unique occurrence. Two of these are the local charge singlets and the third is the interdot spin singlet. In the  $t \rightarrow 0$  limit, these three singlets would combine with the interdot spin triplet to form a sixfold degenerate ground state with  $SU(4)$  symmetry.

### B. Left-right symmetric case, away from half-filling

At small  $t$  the spectra away from half-filling, Fig. 7(a), look similar to those in the single dot limit [44], however a closer look at the subgap states reveals some interesting details, Fig. 7(b). At  $\delta \sim 0.1$  there appears to be a transition

between two different singlet ground states, which is actually a rapid crossover. For  $\delta < 0.1$ , the ground state of a single dot is a spin doublet Shiba state, thus the DQD systems has nearly degenerate singlet and triplet states for low  $t$ . The lowest spectroscopically observable excitations are the two doublet states which decrease in energy  $\Omega$  as  $\delta$  increases; these doublets correspond to one of the QDs having a quasiparticle bound to it. As  $\Omega$  drops below  $0.5\Delta$ , an additional singlet state enters the subgap range. This state can be interpreted as the state where both QDs have one quasiparticle attached each. The ground state for  $\delta > 0.1$  is indeed of this type.

In the crossover region the excited singlet state occurs approximately at the sum of energies of the two doublet Shiba states, thus it is pushed together with these two states to higher energies as  $t$  increases. The spectra for larger  $t$  are shown in Figs. 7(c) and 7(d). Finiteness of excitation energies to the doublet states is confirmed by inspecting the spectrum of the subgap excitations (bottom panel in Fig. 8). Despite the continuous evolution of the ground state as a function of  $\delta$ , its nature is not the same at  $\delta = 0$  as in the large  $|\delta|$  limit, see other panels in Fig. 8. Most notably, the pairing expectation value  $\langle d_{1\uparrow}d_{1\downarrow} \rangle$  has opposite signs. The  $|\delta| \lesssim 0.1$  ground state is the interdot singlet  $|S1\rangle$  formed by unscreened local moments. For  $|\delta| \gtrsim 0.1$ , the ground state is close to  $|S2\rangle$ , which can also be thought of as two separate Kondo compensated states with quasiparticles attached. The energy of  $|S2\rangle$  away from half-filling evolves as  $\approx U - 2\Gamma - \delta^2/\Gamma$ . In the wide-gap limit it thus becomes important at  $\delta$  of order  $\sqrt{U\Gamma}$  which is the charge fluctuation scale in the single-impurity Anderson model. For very large  $\delta$  the dots are unoccupied and play no role, thus the system is a simple BCS superconductor. As expected, the main component of  $|S2\rangle$  for large  $\delta$  is the empty state  $|0\rangle$ .

It may be noted that the singlet ground state for  $\delta \geq 0.1$  is actually similar in nature to the singlet ground state for  $\delta = 0$

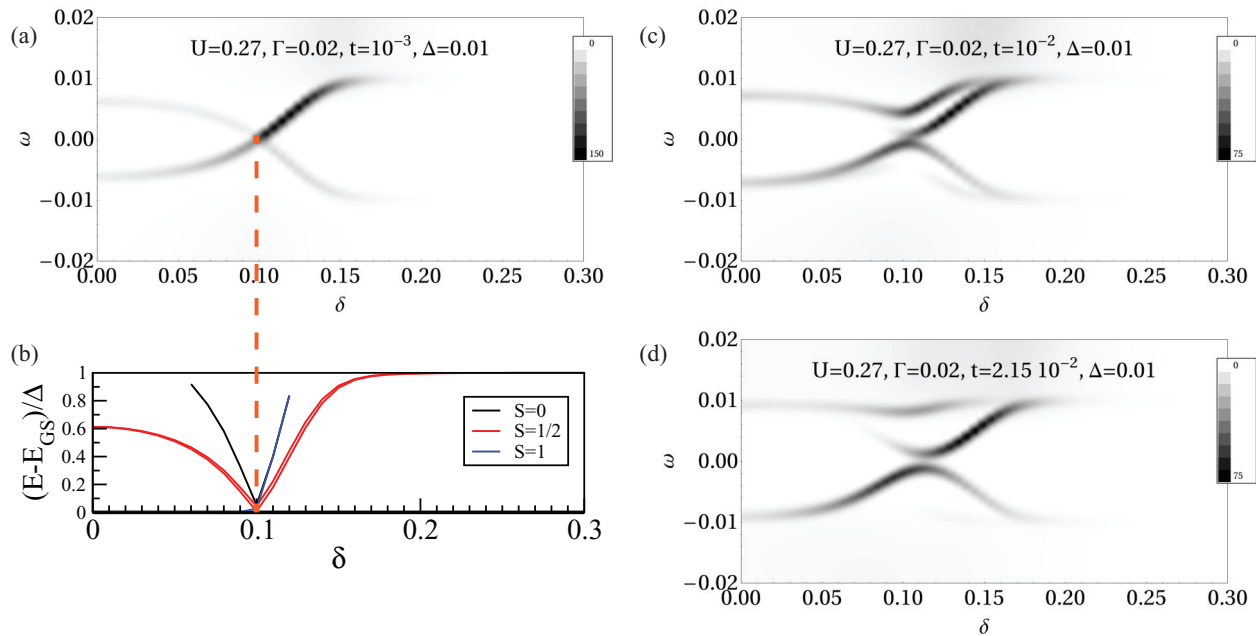


FIG. 7. (Color online) Spectral function  $A_1(\omega)$  in the left-right symmetric DQD system away from half-filling. (a) Small interdot tunneling  $t = 10^{-3}$ . (b) Subgap Shiba state diagram for  $t = 10^{-3}$ . In the range  $\delta \sim 0.1$ , the  $S = 1/2$  and the excited  $S = 0$  state have small but nonzero energy. (c) and (d) Spectra at stronger interdot coupling.

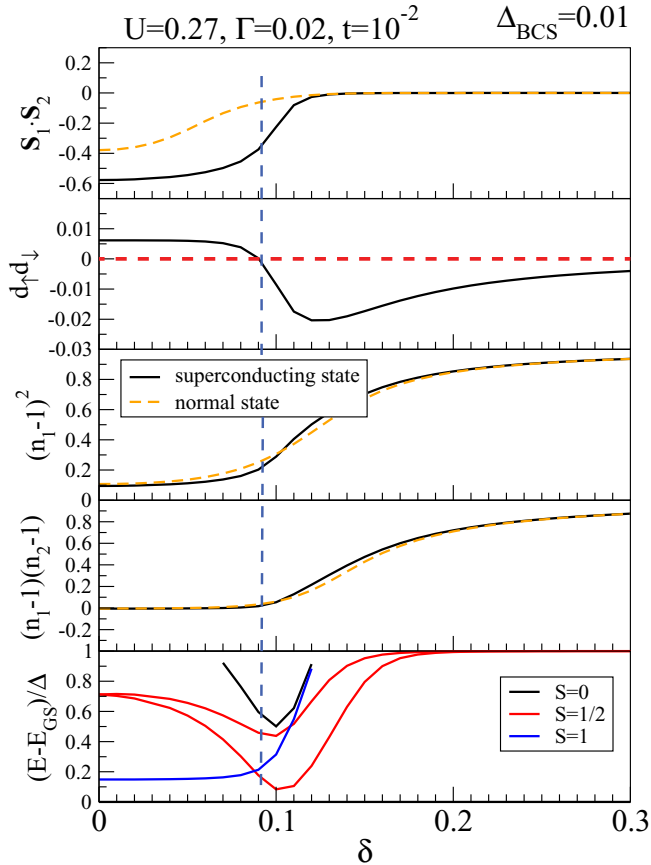


FIG. 8. (Color online) Expectation values in the left-right symmetric DQD system away from half-filling. The value of  $t$  is the same as in Fig. 7(c). Note the position of the triplet state below the excited singlet for  $\delta > 0.1$ .

at  $\Gamma > \Gamma_t$  discussed in the previous subsection. One could draw a phase diagram in the  $(\Gamma/U, \delta/U)$  plane delineating the parameter ranges where the single ground state is either of type  $|S1\rangle$  or  $|S2\rangle$ . In the  $t \rightarrow 0$  limit, this line would be well defined and would, in fact, coincide with the singlet-doublet QPT line of the single QD problem. At  $t \neq 0$ , the QPT is however replaced by a crossover with a width roughly proportional to  $t$ .

### 1. Doublet splitting

While at  $\delta = 0$  the doublet excitations are degenerate, there is a splitting induced by the interdot coupling of order proportional to  $\delta t$ . This can be understood as the formation of molecular orbitals by the quasiparticle attached to the dots and can be understood within the superconducting atomic limit. The eigenvalues of the doublet states are

$$\frac{1}{2} \left( U \pm \left\{ 2(2t^2 + 2\Gamma^2 + \delta_1^2 + \delta_2^2 \pm \sqrt{[4t^2 + (\delta_1 - \delta_2)^2](\delta_1 + \delta_2)^2}) \right\}^{1/2} \right), \quad (17)$$

which for  $\delta = \delta_1 = \delta_2$  simplifies to

$$\frac{U}{2} \pm \sqrt{\Gamma^2 + (t \pm \delta)^2}. \quad (18)$$

(The two  $\pm$  signs in this expression are independent.) For  $t = \delta = 0$  these energies are

$$\frac{U}{2} \pm \Gamma, \quad (19)$$

each being doubly degenerate. These corresponding states are of the form

$$\frac{1}{\sqrt{2}} d_{1\sigma}^\dagger (1 \pm d_{2\uparrow}^\dagger d_{2\downarrow}^\dagger) |0\rangle, \quad (20)$$

and the analogous states with  $1 \leftrightarrow 2$ . The degeneracy is lifted when *both*  $t$  and  $\delta$  are nonzero, the splitting being

$$\frac{2\delta t}{\Gamma} \quad (21)$$

to lowest order in  $t$  and  $\delta$ . This can be interpreted as the bond formation ( $t \neq 0$ ), with bonding-antibonding splitting emerging only away from half-filling ( $\delta \neq 0$ ) in the superconducting case because one-particle and three-particle states are mixed.

For intermediate interdot coupling, see the  $t = 10^{-2}$  case in Fig. 7(c), the splitting of the doublet Shiba states is clearly visible. We notice that the asymmetry of the particlelike ( $\omega > 0$ ) and holelike ( $\omega < 0$ ) transitions exists for both branches. At larger  $t = 2.15 \times 10^{-2}$ , the higher-energy doublet state is already essentially merged with the continuum and is hardly spectroscopically observable. For even larger  $t \sim 0.1$  (not shown) the system is in the molecular orbital regime and the two dots behave as a single large quantum dot which undergoes Kondo screening when  $\delta$  is appropriately tuned and therefore manifests the singlet-doublet transition.

We remark on the decreasing spectral weight of the subgap states as they approach the gap edges at  $\omega = \pm\Delta$ , already observed and discussed for the case of a single quantum dot in Ref. [15]. This is very visible in Fig. 7, as well as in all other spectra in the following, and appears to be a general property. The subgap states always merge with the continuum in such a way that the energy evolves continuously.

### 2. Flux dependence

We now consider the flux dependence at  $\delta \neq 0$ . The main effect for small  $\delta$  and  $t$  is some initial ( $\phi = 0$ ) splitting of the doublet Shiba state, otherwise the results are rather similar to those shown in Fig. 4. For larger  $\delta \approx 0.1$  in the valence fluctuation region, the behavior is more interesting and the flux can induce a quantum phase transition by strongly increasing the splitting between the doublet states, see Fig. 9. This type of the phase transition will be studied in depth in the following sections. Here we comment on some other features: (a) both doublet excitations are now spectroscopically observable, unlike at half-filling, (b) the singlet-triplet splitting is now more significantly affected by nonzero  $\phi$ , and (c) the second singlet state is also significantly  $\phi$  dependent (in fact, the two singlet states merge at  $\phi = \pi$  in the  $t \rightarrow 0$  limit). There is a significant spectral weight redistribution across the phase transition, thus it should be easily experimentally observable.

### 3. V dependence

In the normal state, the interdot capacitive coupling leads to nontrivial effects also at quarter-filling [40,41,43]. For sufficiently large  $V$  (which does not need to be comparable in

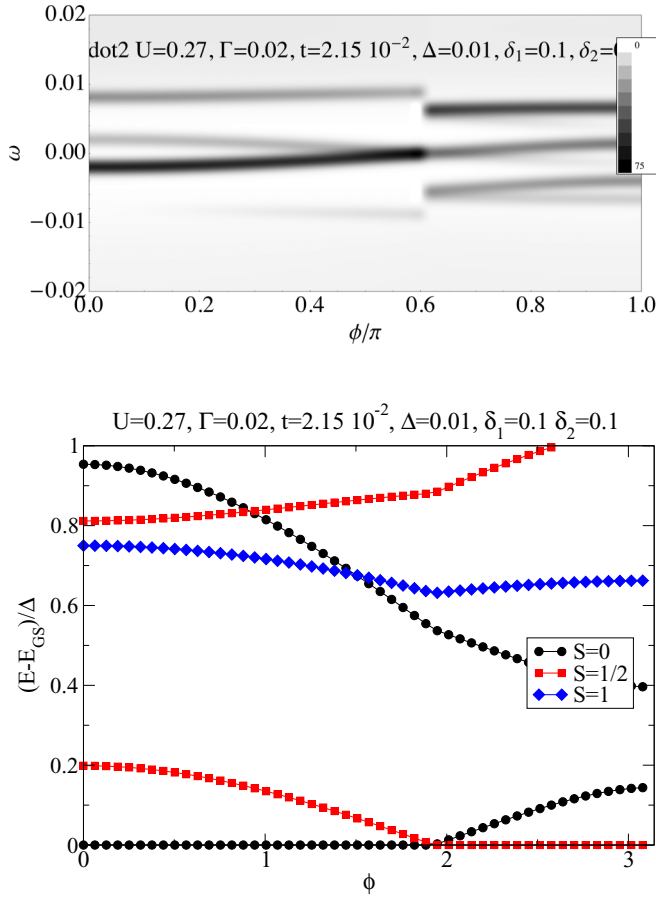


FIG. 9. (Color online) Spectral function  $A(\omega)$  and the diagram of the subgap Shiba states for  $\delta_1 = \delta_2 = 0.1$  as a function of the superconducting phase difference  $\phi$ .

value to  $U$ ), a local moment fixed point emerges in the valence fluctuation range, with the occupancy pinned to one quarter. In this regime, the degeneracy between the  $|0, \uparrow\rangle, |0, \downarrow\rangle, |\uparrow, 0\rangle, |\downarrow, 0\rangle$  states leads to a  $SU(4)$  Kondo effect different from the one at half-filling (which requires fine tuning  $V \approx U$ ). For exact degeneracy, there must be no interdot tunneling, otherwise there is a splitting into bonding and antibonding molecular orbitals and a regular  $SU(2)$  spin Kondo effect is expected.

We find signatures of these effects also in the superconducting case. The results for moderately large  $V/D = 0.1$  are shown in Fig. 10 for two values of interdot tunneling  $t$ . Compared to the  $V = 0$  case, we find a range of  $\delta$  where quarter-filling is stabilized and the ground state is a spin doublet. For  $t = 0$ , both doublets would be degenerate, but at finite  $t$  we find a splitting of order  $t$ . In this range of  $\delta$ , both singlet and triplet Shiba states are spectroscopically visible.

### C. Generic case: Unequal dots

We fix the on-site energy of one of the dots ( $\delta_2$ ) and vary the other ( $\delta_1$ ). We do so for different choices of  $\delta_2$ : at  $\delta_2 = 0$  (dot 2 in the Kondo regime) and  $\delta_2 = 0.1$  (dot 2 in the valence fluctuation regime).

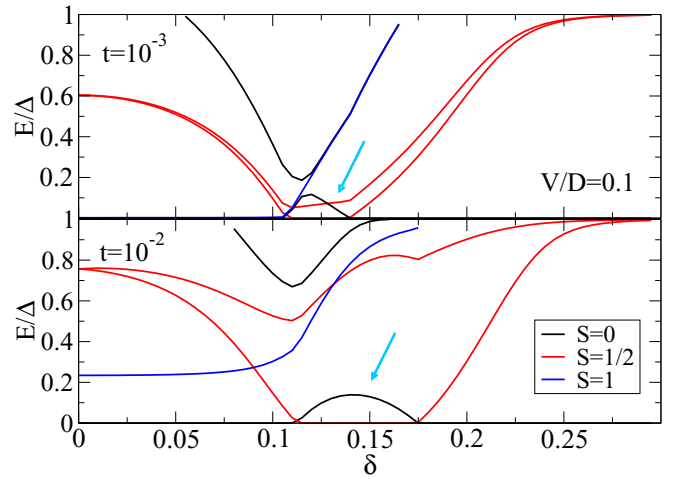


FIG. 10. (Color online) Subgap Shiba state diagram at finite interdot capacitive coupling  $V/D = 0.1$ . Top panel:  $t = 10^{-3}$ , to be compared with Figs. 7(a) and 7(b). Bottom panel:  $t = 10^{-2}$ , to be compared with Figs. 7(c) and 8. The arrows indicate the new feature: a region close to the VF point where the interdot coupling induces a phase transition to the doublet state, corresponding to the emergence of a local moment regime with a single electron in the DQD (quarter-filling).

#### 1. Dot 2 in the Kondo regime

In Fig. 11 we plot the results for  $\delta_2 = 0$ . At small  $t = 10^{-3}$ , top row, the dots are nearly decoupled, thus dot 1 shows the evolution vs  $\delta$  typical of a single QD, while the spectrum on dot 2 shows peaks at constant energy of  $\Omega = 0.6\Delta$ , as expected for  $\delta_2 = 0$ . The interdot effects become visible around  $t = 2 \times 10^{-3}$  in the form of weak features of  $A_1(\omega)$  mirrored in  $A_2(\omega)$ , which then amplify and mix with the Shiba states of dot 2. By  $t = 10^{-2}$ , center row in Fig. 11, the structure of the subgap states is already quite complex and the superexchange  $J$  needs to be invoked to explain all features. The evolution of the spectral weights is nontrivial and discontinuous at the point where the ground state changes from singlet to doublet.

As an aid in the interpretation, we show in Fig. 12 the subgap many-particle spectrum. The transition occurs at  $\delta_1 \approx 0.1$ . For  $\delta_1 < 0.1$ , the spectrum is similar to that in the  $t \rightarrow 0$  limit: the ground state is a singlet, and with increasing  $\delta_1$  one of the doublet states comes down in energy and becomes the new ground state. The effect of nonzero  $t$  is visible in the slightly increasing (vs  $\delta_1$ ) energy of the other doublet state and in the singlet-triplet splitting. The most interesting features occur for  $\delta_1 \gtrsim 0.1$ . The differences between  $A_1(\omega)$  and  $A_2(\omega)$  are notable. In  $A_2(\omega)$ , the most pronounced features correspond to the transitions from the doublet GS to the two excited singlet states, while the transition to the triplet state is not visible at all. In  $A_1(\omega)$ , on the other hand, the dominant feature is the transition from the doublet GS to the *triplet excited state*, while the weights for the transitions to the singlet excited states are much weaker. Since in the atomic limit the triplet state does not depend at all on  $\delta_i$ , nor on  $t$ , and the lowest lying singlet state depends on these parameters only very weakly, the differences between the two spectra are predominantly due to the different site amplitudes of the doublet wave function. The very strong

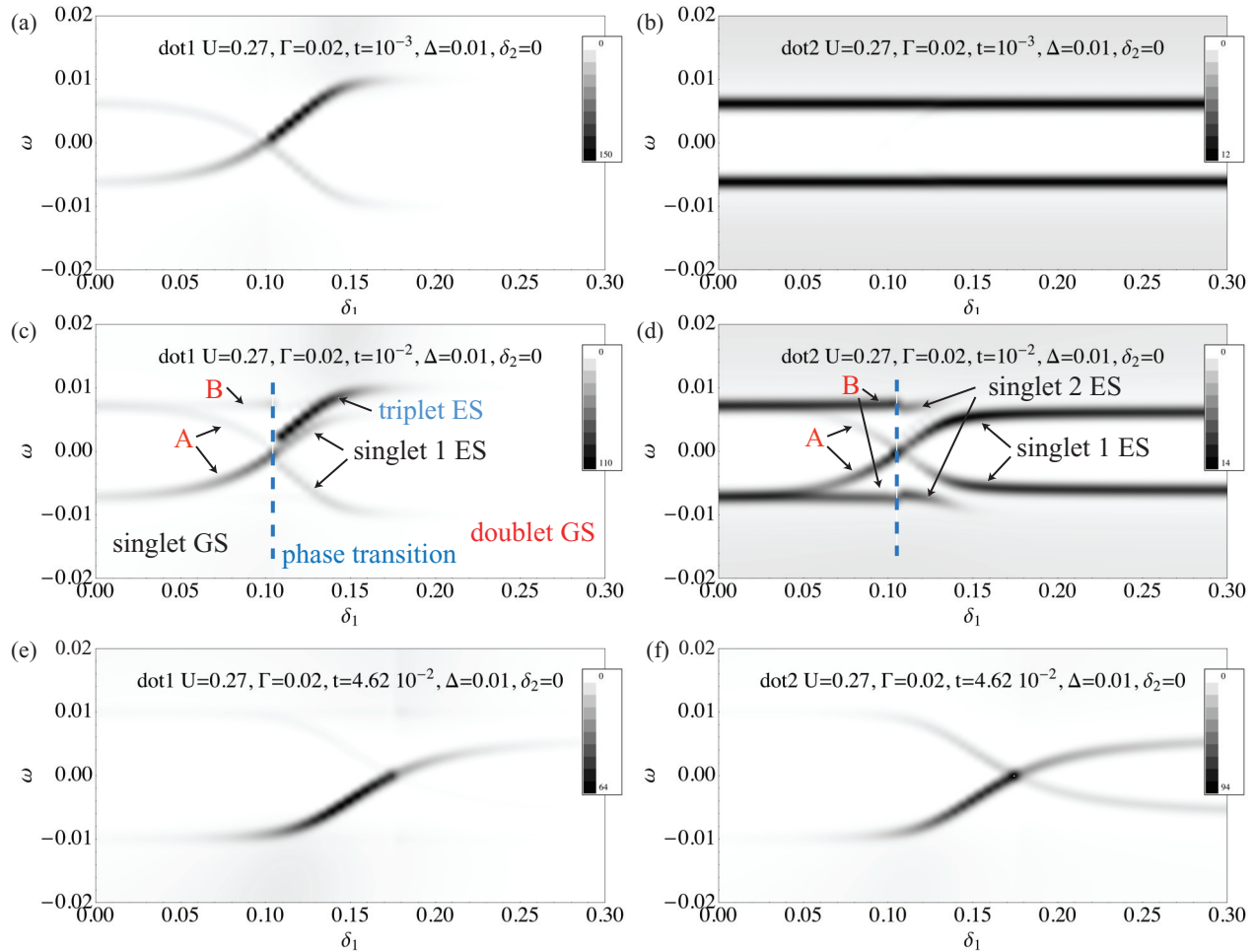


FIG. 11. (Color online) Spectral function on dot 1 (left panels) and dot 2 (right panels) for a range of interdot couplings  $t$ . The quantum dot 2 is kept at  $\delta_2 = 0$ , which is the *Kondo regime*. The arrows mark the different spectroscopically observable excited states (ES).

transition on the particle side ( $\omega > 0$ ) of  $A_1(\omega)$  is due to the charge depletion by high on-site potential which leads to strong enhancement of the matrix element for the particle addition.

For  $\delta_1 \gg 0.1$ , the only resonance remaining inside the gap is that corresponding to the Shiba state on dot 2: it is positioned at  $0.6\Delta$  in the large  $\delta_1$  limit where dot 1 has little effect on dot 2 in the subgap energy range. Other subgap states are pushed into the continuum, since dot 1 no longer has a magnetic moment.

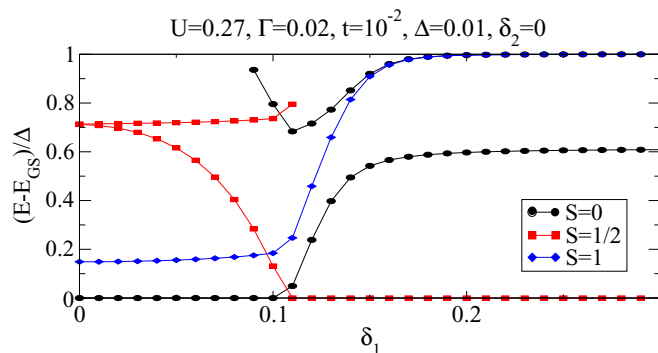


FIG. 12. (Color online) Subgap spectrum corresponding to the center row in Fig. 11.

For large  $t = 4.62 \times 10^{-2}$ , bottom row in Fig. 11, we enter the regime of a single effective QD, thus the variation of the subgap state manifests in a similar way in both spectral functions, except for the differences in spectral weights due to the different on-site energies.

## 2. Dot 2 in the valence fluctuation regime

We now consider the case of  $\delta_2 = 0.1$  where the second quantum dot is in the valence fluctuation regime, see Fig. 13. The symmetry  $\delta_1 \leftrightarrow -\delta_1$  is lost and we need to consider the full range for  $\delta_1$ . The results for  $\delta_1 \sim 0$  have been discussed in the previous subsection (with the roles of  $\delta_1$  and  $\delta_2$  reversed), thus we focus on the cases where  $\delta_1$  is itself in the valence fluctuating range  $|\delta_1| \approx 0.1$ .

For  $\delta_1 > 0$  we find a transition to a doublet ground state at  $\delta_1 \approx 0.14$ . For larger  $\delta_1$ , the excited singlet state remains at low energies, while all other Shiba states move up in energy and merge with the continuum. In this regime, dot 1 is fully depleted, thus the Shiba spectrum is determined by dot 2 which is very close to the occupancy controlled singlet-doublet transition. Consequently, this leads to a spectral resonance very close to  $\omega = 0$  for all  $\delta_1 \gtrsim 0.14$ .

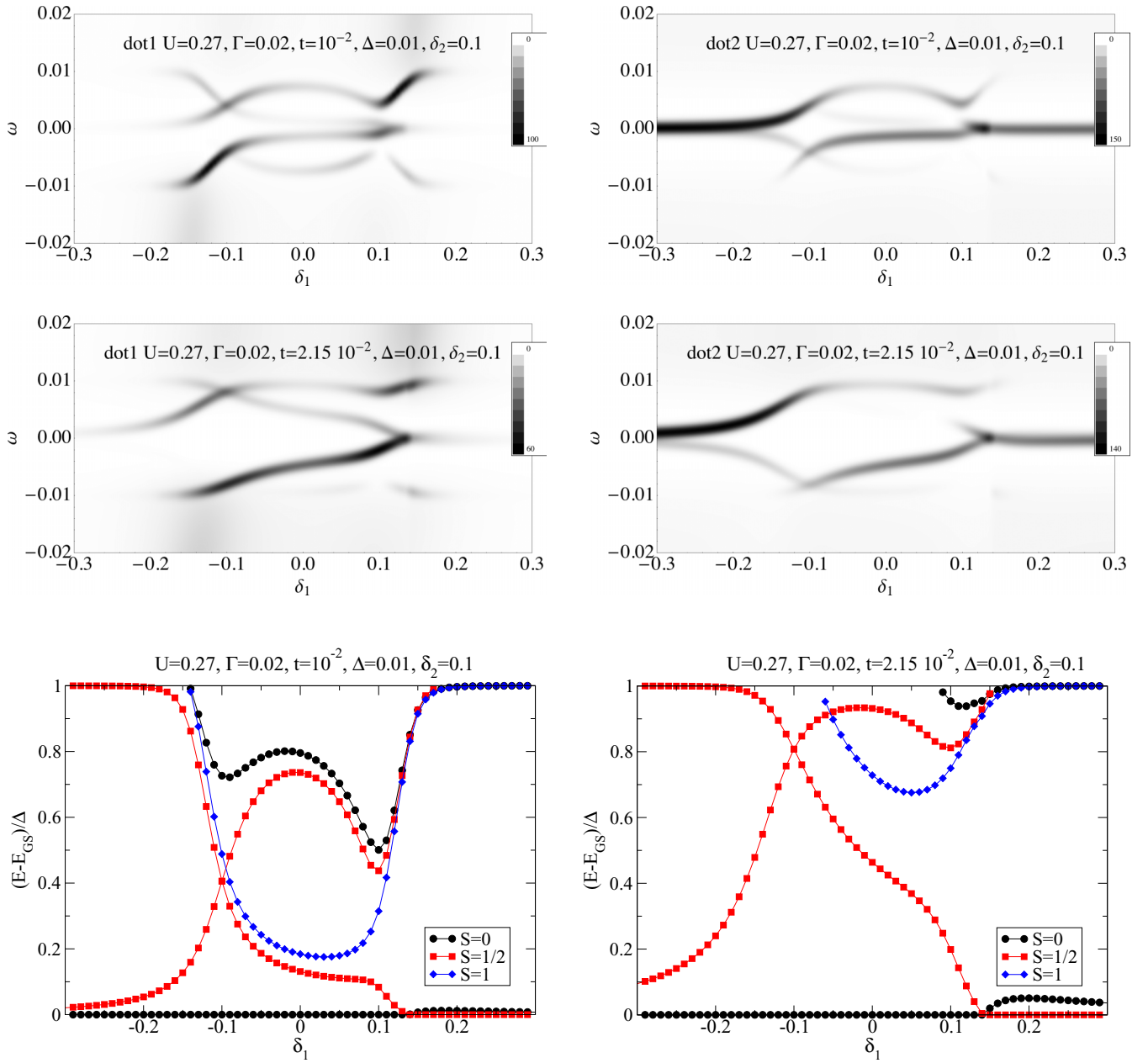


FIG. 13. (Color online) Spectral function on dot 1 (left panels) and dot 2 (right panels) in the *superconducting* state for a range of interdot couplings  $t$ . The quantum dot 2 is kept at  $\delta_2 = 0.1$ , which is the *valence fluctuation regime*. The last row shows the corresponding many-particle Shiba state diagrams.

For  $\delta_1 < 0$ , the behavior is rather different. Dot 1 is progressively filled, moving across the valence fluctuation point at  $\delta_1 = -0.1$ . The ground state is a singlet for all negative  $\delta_1$ , but the doublet excitations undergo an interesting evolution, namely at  $\delta_1 = -0.1$  we find a crossing of two different types of the doublet excitations. This is the same type of degeneracy of the doublet states as found at half-filling in the left-right symmetric problems. The level crossing is thus a sign of a symmetry which is established at  $\delta_1 = -\delta_2$ , namely a combination of reflection and particle-hole transformation, which leaves the Hamiltonian invariant. Again, there is a spectral peak close to  $\omega = 0$  for  $\delta_1 < -0.1$ . In this case, the residual coupling to dot 2 leads to a different order of Shiba

states, i.e., the ground state is a doublet, while the excited state is a singlet. For large negative  $\delta_1$  this order should eventually be reversed again, because the excitation spectra for  $\delta_1 \rightarrow \pm\infty$  are expected to be the same.

Finally, we briefly discuss the results for the case where one of the dots (dot 2, for definitiveness) is driven to the empty orbital regime by tuning  $\delta_2$  to a large value well above  $U/2 + \Gamma \approx 0.15$ . The system then essentially behaves as a single quantum dot; this includes also the level diagram of the Shiba states. Even though dot 2 is unoccupied, at finite interdot coupling there are still some faint features from  $A_1(\omega)$  being mirrored into the spectral function  $A_2(\omega)$  (results not shown). As  $t$  grows one can smoothly reach the regime of molecular

orbitals. To conclude, for large  $\delta_2$  the DQD always effectively behaves as a single quantum dot: for small  $t$ , the effective dot is the physical QD 1, and for large  $t$  it is the “large” QD made of molecular orbitals spanning both dots. These two regimes are smoothly connected.

#### IV. TWO-IMPURITY KONDO “CRITICALITY”

In the DQD with normal-state leads the low-temperature physics is governed by the two-impurity Kondo effect. The non-Fermi-liquid (NFL) fixed point of this model is never actually reached because the particle exchange between the leads is a relevant perturbation (in the renormalization group sense) [73], but its presence still has important effects in a wide parameter range. In Sec. III B we observed that at half-filling the ground state is the same singlet many-particle state for any value of  $t$ ; this is the case for any  $\Gamma/U$  ratio. This continuity is the superconducting counterpart of the crossover behavior found in the normal state. The presence of the two-impurity Kondo model fixed point is thus only felt through the nontrivial evolution of the expectation values, in particular that of the spin-spin correlation function  $\langle \mathbf{S}_1 \cdot \mathbf{S}_2 \rangle(t)$ .

The NFL fixed point can be approached in the normal state arbitrarily closely if the particle exchange between the two channels is suppressed while the magnetic exchange coupling is maintained [73]. We consider here how this scenario manifests in the superconducting case through the properties of the subgap states. The interdot coupling term in the Hamiltonian is thus replaced by

$$H_{12} = J \mathbf{S}_1 \cdot \mathbf{S}_2, \quad (22)$$

where  $\mathbf{S}_i$  are the spin operators of the impurities.

The results are shown in Fig. 14 for a value of  $\Gamma/U$  in the suitable range for a competition between the singlet ground states (a) consisting of two separate Kondo clouds and (b) intersite singlet generated by the superexchange coupling  $4t^2/U$ . We indeed observe a genuine quantum phase transition (level crossing) between the two singlets at  $J = J_c \approx 1.1 \times 10^{-3}$ . State (a) is characterized by near-zero spin correlations  $\langle \mathbf{S}_1 \cdot \mathbf{S}_2 \rangle \approx 0$ , while state (b) is an intersite

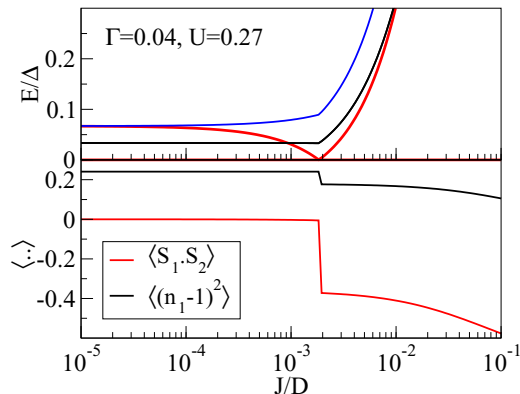


FIG. 14. (Color online) Two-impurity Kondo effect manifesting through the quantum phase transition between two different many-particle subgap singlet states in the model with exchange coupling  $J$  between the dots and no particle transfer ( $t = 0$ ).

singlet state with large spin-spin values. All other system properties also change discontinuous across the transition [see the example of the charge fluctuations  $\langle (n_1 - 1)^2 \rangle$  also shown in Fig. 14].

The excited singlet subgap state is not directly spectroscopically observable in tunneling experiments. Nevertheless, the phase transition does manifest as a visible spectral discontinuity: there is a kink in the energy of the doublet excitation, and the spectral weights have a jump (results not shown). Alternatively, the radio-frequency spectroscopy could be used [34]. The two-impurity Kondo effect quantum phase transition is thus in principle spectroscopically observable, if only a system with sufficiently suppressed particle exchange could be physically realized [73].

This section may be concluded with the following observation: In the normal-state case, the two-impurity Kondo quantum phase transition is a second-order transition with true quantum criticality, while in the superconducting case it is a first-order transition (i.e., level crossing between two subgap singlet states that are separated from the quasiparticle continuum). An interesting question for future work is to explore the structure of the excitations in the continuum above  $\Delta$ : Are the Bogolioubov states formed out of Fermi liquid or non-Fermi liquid quasiparticles? For  $\Delta < T_K^{2IK}$ , the latter should be the case.

#### V. CONCLUSION

Double quantum dots are described by impurity models with properties controlled by a number of fixed points. To each fixed point (regime) it is possible to associate particular features observed in the subgap spectra. In this work double dots were studied with a quantitatively accurate method focusing on the regimes of strong dependence on model parameters that could be targeted by future experiments. Qualitative trends can be reproduced in the superconducting atomic limit which projects out the continua of the quasiparticle states above  $\Delta$  by taking the  $\Delta \rightarrow \infty$  limit, while for quantitative correctness it is crucial to use a nonperturbative technique such as the NRG, especially in the regimes where the Kondo effect plays an important role.

We now summarize the main experimentally verifiable predictions of this work:

(1) The Kondo, antiferromagnetic, and molecular-orbital regimes at half-filling can be distinguished by the features in the spectral function both inside and outside the gap.

(2) The splitting of the doublet excited states induced by the flux (difference of superconducting phases) is only visible away from half-filling and is proportional to the interdot coupling.

(3) In the large hybridization regime, the interdot triplet state has lower energy than the interdot singlet state due to the level repulsion between the singlet Shiba states.

(4) At half-filling, the interdot capacitive coupling leads to a crossover at  $V \sim U$  between spin-singlet and charge-singlet regimes.

(5) At quarter-filling, the interdot capacitive coupling generates a quantum phase transition to a doublet ground state which corresponds to the local-moment fixed point with

fourfold degeneracy in the  $t \rightarrow 0$  limit (finite  $t$  leads to a splitting of the doublet states).

(6) By tuning one dot to the Kondo regime and the other to the valence fluctuation regime, the ground state becomes a doublet and both singlet and triplet excitations can be observed: the triplet state have high spectral weight on the valence fluctuating dots, while the singlet state is better observed on the half-filled dot in the Kondo regime.

(7) By tuning both dots to the valence fluctuation regime, one fluctuating between zero and single occupancy, the other between double and single occupancy, the system has combined reflection and particle-hole transformation symmetry, leading to a crossing of the excited doublet states.

The transitions which change the spin by  $1/2$  are directly observable in tunneling spectroscopy, while radio-frequency spectroscopy would uncover further transitions. It should be stressed that some of the most interesting features are present (or become observable) only away from half-filling. The valence fluctuation and local moment regimes near quarter-filling are just as intriguing, if not more, as the Kondo regime at half-filling.

#### ACKNOWLEDGMENT

I acknowledge the support of the Slovenian Research Agency (ARRS) under Program No. P1-0044.

- 
- [1] I. Giaever, Energy gap in superconductors measured by electron tunneling, *Phys. Rev. Lett.* **5**, 147 (1960).
- [2] I. Giaever, Electron tunneling and superconductivity, *Rev. Mod. Phys.* **46**, 245 (1974).
- [3] S. H. Pan, E. W. Hudson, K. M. Lang, H. Eisaki, S. Uchida, and J. C. Davis, Imaging the effects of individual zinc impurity atoms on superconductivity in  $\text{Bi}_2\text{Sr}_2\text{CaCu}_2\text{O}_{8+\delta}$ , *Nature (London)* **403**, 746 (2000).
- [4] A. V. Balatsky, I. Vekhter, and J.-X. Zhu, Impurity-induced states in conventional and unconventional superconductors, *Rev. Mod. Phys.* **78**, 373 (2006).
- [5] S. H. Ji, T. Zhang, Y. S. Fu, X. Chen, X.-C. Ma, J. Li, W.-H. Duan, J.-F. Jia, and Q.-K. Xue, High-resolution scanning tunneling spectroscopy of magnetic impurity induced bound states in the superconducting gap of Pb thin films, *Phys. Rev. Lett.* **100**, 226801 (2008).
- [6] M. Iavarone, G. Karapetrov, J. Fedor, D. Rosenmann, T. Nishizaki, and N. Kobayashi, The local effect of magnetic impurities on superconductivity in  $\text{Co}_x\text{NbSe}_2$  and  $\text{Mn}_x\text{NbSe}_2$  single crystals, *J. Phys.: Condens. Matter* **22**, 015501 (2010).
- [7] S.-H. Ji, T. Zhang, Y.-S. Fu, X. Chen, J.-F. Jia, Q.-K. Xue, and X.-C. Ma, Application of magnetic atom induced bound states in superconducting gap for chemical identification of single magnetic atoms, *Appl. Phys. Lett.* **96**, 073113 (2010).
- [8] K. J. Franke, G. Schulze, and J. I. Pascual, Competition of superconductivity phenomena and Kondo screening at the nanoscale, *Science* **332**, 940 (2011).
- [9] M. Ruby, F. Pientka, Y. Peng, F. von Oppen, B. W. Heinrich, and K. J. Franke, Tunneling processes into localized subgap states in superconductors, [arXiv:1502.05048](https://arxiv.org/abs/1502.05048).
- [10] A. C. Hewson, *The Kondo Problem to Heavy-Fermions* (Cambridge University Press, Cambridge, 1993).
- [11] H. Shiba, Classical spins in superconductors, *Prog. Theor. Phys.* **40**, 435 (1968).
- [12] A. Sakurai, Comments on superconductors with magnetic impurities, *Prog. Theor. Phys.* **44**, 1472 (1970).
- [13] J. Zittartz and E. Müller-Hartmann, Theory of magnetic impurities in superconductors. I. Exact solution of the Nagaoka equations, *J. Phys.* **232**, 11 (1970).
- [14] M.-S. Choi, M. Lee, K. Kang, and W. Belzig, Kondo effect and Josephson current through a quantum dot between two superconductors, *Phys. Rev. B* **70**, 020502 (2004).
- [15] J. Bauer, A. Oguri, and A. C. Hewson, Spectral properties of locally correlated electrons in a Bardeen-Cooper-Schrieffer superconductor, *J. Phys.: Condens. Matter* **19**, 486211 (2007).
- [16] C. Karrasch, A. Oguri, and V. Meden, Josephson current through a single Anderson impurity coupled to BCS leads, *Phys. Rev. B* **77**, 024517 (2008).
- [17] C. P. Moca, E. Demler, B. Jankó, and G. Zaránd, Spin-resolved spectra of Shiba multiplets from Mn impurities in  $\text{MgB}_2$ , *Phys. Rev. B* **77**, 174516 (2008).
- [18] T. Meng, S. Florens, and P. Simon, Self-consistent description of Andreev bound states in Josephson quantum dot devices, *Phys. Rev. B* **79**, 224521 (2009).
- [19] S. De Franceschi, L. Kouwenhoven, C. Schenberger, and W. Wernsdorfer, Hybrid superconductor-quantum dot devices, *Nat. Nanotechnol.* **5**, 703 (2010).
- [20] R. Maurand, T. Meng, E. Bonet, S. Florens, L. Marty, and W. Wernsdorfer, First-order  $0-\pi$  quantum phase transition in the Kondo regime of a superconducting carbon-nanotube quantum dot, *Phys. Rev. X* **2**, 011009 (2012).
- [21] J.-D. Pillet, C. H. L. Quay, P. Morin, C. Bena, A. Levy Yeyati, and P. Joyez, Andreev bound states in supercurrent-carrying carbon nanotubes revealed, *Nat. Phys.* **6**, 965 (2010).
- [22] E. J. H. Lee, X. Jiang, M. Houzet, R. Aguado, C. M. Lieber, and S. De Franceschi, Spin-resolved Andreev levels and parity crossings in hybrid superconductor-semiconductor nanostructures, *Nat. Nanotech.* **9**, 79 (2014).
- [23] J.-D. Pillet, P. Joyez, R. Žitko, and M. F. Goffman, Tunneling spectroscopy of a single quantum dot coupled to a superconductor: From Kondo ridge to Andreev bound states, *Phys. Rev. B* **88**, 045101 (2013).
- [24] A. Martín-Rodero and A. Levy Yeyati, Josephson and Andreev transport through quantum dots, *Adv. Phys.* **60**, 899 (2011).
- [25] A. Georges and Y. Meir, Electronic correlations in transport through coupled quantum dots, *Phys. Rev. Lett.* **82**, 3508 (1999).
- [26] R. Aguado and D. C. Langreth, Out-of-equilibrium Kondo effect in double quantum dots, *Phys. Rev. Lett.* **85**, 1946 (2000).
- [27] T. Aono and M. Eto, Kondo effect in coupled quantum dots under magnetic fields, *Phys. Rev. B* **64**, 073307 (2001).
- [28] R. López, R. Aguado, and G. Platero, Nonequilibrium transport through double quantum dots: Kondo effect versus antiferromagnetic coupling, *Phys. Rev. Lett.* **89**, 136802 (2002).
- [29] P. Simon, R. López, and Y. Oreg, Ruderman-Kittel-Kasuya-Yosida and magnetic-field interactions in coupled Kondo quantum dots, *Phys. Rev. Lett.* **94**, 086602 (2005).

- [30] M. Lee, M.-S. Choi, R. Lopez, R. Aguado, J. Martinek, and R. Žitko, The two-impurity Anderson model revisited: Competition between Kondo effect and reservoir-mediated superexchange in double quantum dots, *Phys. Rev. B* **81**, 121311(R) (2010).
- [31] F. S. Bergeret, A. Yeyati, and A. Martín-Rodero, Interplay between Josephson effect and magnetic interactions in double quantum dots, *Phys. Rev. B* **74**, 132505 (2006).
- [32] R. Žitko, M. Lee, R. Lopez, R. Aguado, and M.-S. Choi, Josephson current in strongly correlated double quantum dots, *Phys. Rev. Lett.* **105**, 116803 (2010).
- [33] R. Žitko, O. Bodensiek, and Th. Pruschke, Magnetic anisotropy effects on quantum impurities in superconducting host, *Phys. Rev. B* **83**, 054512 (2011).
- [34] N. Y. Yao, C. P. Moca, I. Weymann, J. D. Sau, M. D. Lukin, E. A. Demler, and G. Zarand, Phase diagram and excitations of a Shiba molecule, *Phys. Rev. B* **90**, 241108(R) (2014).
- [35] M. R. Galpin, D. E. Logan, and H. R. Krishnamurthy, Quantum phase transition in capacitively coupled double quantum dot, *Phys. Rev. Lett.* **94**, 186406 (2005).
- [36] M. R. Galpin, D. E. Logan, and H. R. Krishnamurthy, Dynamics of capacitively coupled double quantum dots, *J. Phys.: Condens. Matter* **18**, 6571 (2006).
- [37] J. Mravlje, A. Ramšak, and T. Rejec, Kondo effect in double quantum dots with interdot repulsion, *Phys. Rev. B* **73**, 241305(R) (2006).
- [38] Y. Okazaki, S. Sasaki, and K. Muraki, Spin-orbital Kondo effect in a parallel double quantum dot, *Phys. Rev. B* **84**, 161305 (2011).
- [39] Y. Nishikawa, A. C. Hewson, D. J. G. Crow, and J. Bauer, Analysis of low-energy response and possible emergent SU(4) Kondo state in a double quantum dot, *Phys. Rev. B* **88**, 245130 (2013).
- [40] S. Amasha, A. J. Keller, I. G. Rau, A. Carmi, J. A. Katine, H. Shtrikman, Y. Oreg, and D. Goldhaber-Gordon, Pseudospin-resolved transport spectroscopy of the Kondo effect in a double quantum dot, *Phys. Rev. Lett.* **110**, 046604 (2013).
- [41] D. A. Ruiz-Tijerina, E. Vernek, and S. E. Ulloa, Capacitive interactions and Kondo effect tuning in double quantum impurity systems, *Phys. Rev. B* **90**, 035119 (2014).
- [42] A. J. Keller, S. Amasha, I. Weymann, C. P. Moca, I. G. Rau, J. A. Katine, H. Shtrikman, G. Zarand, and D. Goldhaber-Gordon, Emergent SU(4) Kondo physics in a spin charge-entangled double quantum dot, *Nat. Phys.* **10**, 145 (2014).
- [43] M. Filippone, C. P. Moca, G. Zarand, and C. Mora, Kondo temperature of SU(4) symmetric quantum dots, *Phys. Rev. B* **90**, 121406 (2014).
- [44] See Supplemental Material at <http://link.aps.org/supplemental/10.1103/PhysRevB.91.165116> for reference results for the single quantum dot problem in the superconducting case, as well as the double quantum dot problem in the normal-state case, and some details on the superconducting atomic limit.
- [45] H. R. Krishnamurthy, J. W. Wilkins, and K. G. Wilson, Renormalization-group approach to the Anderson model of dilute magnetic alloys. I. Static properties for the symmetric case, *Phys. Rev. B* **21**, 1003 (1980).
- [46] K. G. Wilson, The renormalization group: Critical phenomena and the Kondo problem, *Rev. Mod. Phys.* **47**, 773 (1975).
- [47] H. R. Krishnamurthy, J. W. Wilkins, and K. G. Wilson, Renormalization-group approach to the Anderson model of dilute magnetic alloys. II. Static properties for the asymmetric case, *Phys. Rev. B* **21**, 1044 (1980).
- [48] K. Satori, H. Shiba, O. Sakai, and Y. Shimizu, Numerical renormalization group study of magnetic impurities in superconductors, *J. Phys. Soc. Jpn.* **61**, 3239 (1992).
- [49] O. Sakai, Y. Shimizu, H. Shiba, and K. Satori, Numerical renormalization group study of magnetic impurities in superconductors. II. Dynamical excitations spectra and spatial variation of the order parameter, *J. Phys. Soc. Jpn.* **62**, 3181 (1993).
- [50] T. Yoshioka and Y. Ohashi, Ground state properties and localized excited states around a magnetic impurity described by the anisotropic *s-d* interaction in superconductivity, *J. Phys. Soc. Jpn.* **67**, 1332 (1998).
- [51] T. Yoshioka and Y. Ohashi, Numerical renormalization group studies on single impurity Anderson model in superconductivity: A unified treatment of magnetic, nonmagnetic impurities, and resonance scattering, *J. Phys. Soc. Jpn.* **69**, 1812 (2000).
- [52] A. Oguri, Y. Tanaka, and A. C. Hewson, Quantum phase transition in a minimal model for the Kondo effect in a Josephson junction, *J. Phys. Soc. Jpn.* **73**, 2494 (2004).
- [53] T. Hecht, A. Weichselbaum, J. von Delft, and R. Bulla, Numerical renormalization group calculation of near-gap peaks in spectral functions of the Anderson model with superconducting leads, *J. Phys. Condens. Matter* **20**, 275213 (2008).
- [54] R. Bulla, T. Costi, and T. Pruschke, The numerical renormalization group method for quantum impurity systems, *Rev. Mod. Phys.* **80**, 395 (2008).
- [55] J. S. Lim and M.-S. Choi, Andreev bound states in the Kondo quantum dots coupled to superconducting leads, *J. Phys.: Condens. Matter* **20**, 415225 (2008).
- [56] R. S. Deacon, Y. Tanaka, A. Oiwa, R. Sakano, K. Yoshida, K. Shibata, K. Hirakawa, and S. Tarucha, Interplay of Kondo and superconducting correlations in the nonequilibrium Andreev transport through a quantum dot, *Phys. Rev. Lett.* **104**, 076805 (2010).
- [57] A. Martín-Rodero and A. Levy Yeyati, The Andreev states of a superconducting quantum dot: Mean field versus exact numerical results, *J. Phys.: Condens. Matter* **24**, 385303 (2012).
- [58] A. Kumar, M. Gaim, D. Steininger, A. Levy Yeyati, A. Martín-Rodero, A. K. Hüttl, and C. Strunk, Temperature dependence of Andreev spectra in a superconducting carbon nanotube quantum dot, *Phys. Rev. B* **89**, 075428 (2014).
- [59] W. C. Oliveira and L. N. Oliveira, Generalized numerical renormalization-group method to calculate the thermodynamical properties of impurities in metals, *Phys. Rev. B* **49**, 11986 (1994).
- [60] J. B. Silva, W. L. C. Lima, W. C. Oliveira, J. L. N. Mello, L. N. Oliveira, and J. W. Wilkins, Particle-hole asymmetry in the two-impurity Kondo model, *Phys. Rev. Lett.* **76**, 275 (1996).
- [61] C. A. Paula, M. F. Silva, and L. N. Oliveira, Low-energy spectral density for the Alexander-Anderson model, *Phys. Rev. B* **59**, 85 (1999).
- [62] V. L. Campo and L. N. Oliveira, Alternative discretization in the numerical renormalization group, *Phys. Rev. B* **72**, 104432 (2005).
- [63] W. Hofstetter, Generalized numerical renormalization group for dynamical quantities, *Phys. Rev. Lett.* **85**, 1508 (2000).
- [64] R. Žitko, J. S. Lim, R. Lopez, and R. Aguado, Shiba states and zero-bias anomalies in the hybrid normal-superconductor Anderson model, *Phys. Rev. B* **91**, 045441 (2015).

- [65] V. Koerting, B. M. Andersen, K. Flensberg, and J. Paaske, Nonequilibrium transport via spin-induced subgap states in superconductor/quantum dot/normal metal cotunnel junctions, *Phys. Rev. B* **82**, 245108 (2010).
- [66] Y. Yamada, Y. Tanaka, and N. Kawakami, Interplay of Kondo and superconducting correlations in the nonequilibrium Andreev transport through a quantum dot, *Phys. Rev. B* **84**, 075484 (2011).
- [67] A. Koga, Quantum Monte Carlo study of nonequilibrium transport through a quantum dot coupled to normal and superconducting leads, *Phys. Rev. B* **87**, 115409 (2013).
- [68] A. V. Rozhkov and D. P. Arovas, Interacting-impurity Josephson junction: Variational wave functions and slave-boson mean-field theory, *Phys. Rev. B* **62**, 6687 (2000).
- [69] E. Vecino, A. Martín-Rodero, and A. Yeyati, Josephson current through a correlated quantum level: Andreev states and  $\pi$  junction behavior, *Phys. Rev. B* **68**, 035105 (2003).
- [70] F. Bergeret, A. Yeyati, and A. Martín-Rodero, Josephson effect through a quantum dot array, *Phys. Rev. B* **76**, 174510 (2007).
- [71] J. Mravlje, A. Ramšak, and T. Rejec, Conductance of deformable molecules with interaction, *Phys. Rev. B* **72**, 121403(R) (2005).
- [72] R. Žitko and J. Bonča, Multi-impurity Anderson model for quantum dots coupled in parallel, *Phys. Rev. B* **74**, 045312 (2006).
- [73] G. Zaránd, C.-H. Chung, P. Simon, and M. Vojta, Quantum criticality in a double quantum-dot system, *Phys. Rev. Lett.* **97**, 166802 (2006).